Hamiltonian symmetries in auxiliary-field quantum Monte Carlo calculations for electronic structure

Mario Motta, Shiwei Zhang, and Garnet Kin-Lic Chan

Hamiltonian symmetries in auxiliary-field quantum Monte Carlo calculations for electronic structure

Mario Motta,[1] Shiwei Zhang,[2,3] and Garnet Kin-Lic Chan[1]

[1] *Division of Chemistry and Chemical Engineering, California Institute of Technology, Pasadena, CA 91125, USA*
[2] *Center for Computational Quantum Physics, Flatiron Institute, New York, NY 10010, USA*
[3] *Department of Physics, College of William and Mary, Williamsburg, VA 23187-8795, USA*

We describe how to incorporate symmetries of the Hamiltonian into auxiliary-field quantum Monte Carlo (AFQMC) calculations. Focusing on the case of Abelian symmetries, we show that the computational cost of most steps of an AFQMC calculation is reduced by N_k^{-1}, where N_k is the number of irreducible representations of the symmetry group. We apply the formalism to a molecular system as well as to several crystalline solids. In the latter case, the lattice translational group provides increasing savings as the number of k points is increased, which is important in enabling calculations that approach the thermodynamic limit. The extension to non-Abelian symmetries is briefly discussed.

I. INTRODUCTION

The basic task of electronic structure (ES) theory is to solve the time-independent Schrödinger equation $\hat{H}|\Psi_\mu\rangle = E_\mu|\Psi_\mu\rangle$, to determine the eigenvalues E_μ and eigenstates $|\Psi_\mu\rangle$ of a Hamiltonian $\hat{H}$. When relativistic effects and nuclear motion are neglected, the second-quantized Born-Oppenheimer Hamiltonian operator has the form [1–3],

$$\hat{H} = \sum_{pq} h_{pq}\hat{a}_p^\dagger\hat{a}_q + \frac{1}{2}\sum_{pqrs}(pr|qs)\,\hat{a}_p^\dagger\hat{a}_q^\dagger\hat{a}_s\hat{a}_r \ ,$$

$$h_{pq} = \int d\mathbf{r}\,\varphi_p^*(\mathbf{r})\left(-\frac{\nabla^2}{2} - \sum_\alpha \frac{Z_a}{|\mathbf{r}-\mathbf{R}_\alpha|}\right)\varphi_q(\mathbf{r}) \ ,$$

$$(pr|qs) = \int d\mathbf{r}\,d\mathbf{r}'\,\varphi_p^*(\mathbf{r})\varphi_r(\mathbf{r})\,\frac{1}{|\mathbf{r}-\mathbf{r}'|}\,\varphi_q^*(\mathbf{r}')\varphi_s(\mathbf{r}') \ ,$$

$$(1)$$

expressed here in atomic units, using a basis of M spin-orbitals $\{\varphi_p\}_{p=1}^M$ for the one-electron Hilbert space. In Eq. (1), α labels nuclei with positions $\mathbf{R}_\alpha$, and $\mathbf{r}, \mathbf{r}'$ denote electronic coordinates.

Many ES methods take advantage of Hamiltonian symmetries [3–8] to improve the efficiency of calculations. In the present work, we give an instructional account of how to incorporate symmetry into the auxiliary-field quantum Monte Carlo (AFQMC) method [9–17] through symmetry adapted orbitals [3, 4]. We illustrate the formalism through the use of reflection symmetry in molecules and lattice translational symmetry in periodic solids. In the case of lattice translational symmetry, the symmetry orbitals become crystalline orbitals, and thus the AFQMC calculation is carried out in a similar framework to other recent implementations of quantum chemical many-body methods in crystals [7, 8, 18–22]. This use of translational symmetry should be distinguished from twist averaging [23–26], as incorporating larger translational groups reduces many-body size effects, rather than only the one-body size effects captured by twist averaging.

The remainder of the paper is structured as follows. In Section II we briefly review the connection between Hamiltonian symmetries, matrix element sparsity, and the AFQMC formalism. We then describe in detail how to use Hamiltonian symmetries to decrease the cost of the various operations involved in an AFQMC calculation. In Section IV we apply the formalism to a test molecule, using reflection symmetries, and crystalline solids, with increasing sizes of the translational group. Conclusions are drawn in Section V. Further implementation details are provided in the Appendices.

II. BACKGROUND

A transformation operator $\hat{s}$ is a symmetry operator for a Hamiltonian $\hat{H}$ if the latter is invariant under the transformation $\hat{s}$,

$$[\hat{s}, \hat{H}] = 0 \quad . \tag{2}$$

The set of operators $\hat{s}$ for which (2) holds forms a group $\mathcal{S}$ under composition, termed the symmetry group of $\hat{H}$. Here, we will focus on Abelian symmetries, i.e. we will assume $[\hat{s}_1, \hat{s}_2] = 0$ for all $\hat{s}_1, \hat{s}_2 \in \mathcal{S}$.

A. Hamiltonian symmetries and sparsity

In the one-electron Hilbert space, the action of symmetry transformations is captured by one-body operators

$$\hat{\Gamma}(\mathbf{s})|\varphi_p\rangle = \sum_r \Gamma(\mathbf{s})_{rp}|\varphi_r\rangle \quad , \tag{3}$$

where $\Gamma(\mathbf{s})_{pr}$ is an M-dimensional matrix representation of $\hat{\Gamma}(\mathbf{s}) \in \mathcal{S}$.

To make the abstract group transformations $\hat{s}$ more concrete, and amenable to storage and numerical manipulation, it is useful to employ the structure theorem for

finitely generated Abelian groups [27–29], which states that $\mathcal{S}$ is isomorphic to a direct product

$$\mathcal{S} \simeq \mathbb{Z}_{n_0} \times \cdots \times \mathbb{Z}_{n_{r-1}} \equiv \mathbb{Z}_{\mathcal{S}} \quad , \quad \prod_{i=0}^{r-1} n_i = |\mathcal{S}| \quad , \quad (4)$$

of cyclic groups $\mathbb{Z}_{n_i}$, of orders n_i multiplying to the number $|\mathcal{S}|$ of elements of $\mathcal{S}$. In what follows, symmetries $\hat{s} \in \mathcal{S}$ will be labeled with strings $\mathbf{s} \in \mathbb{Z}_{\mathcal{S}}$, and sums of such strings will be understood to be modulo the orders n_i of the cyclic groups,

$$\mathbf{s} + \mathbf{t} = (s_0 + t_0 \bmod n_0 \ldots s_{r-1} + t_{r-1} \bmod n_{r-1}) . (5)$$

As detailed in Appendix A 1, from the properties of the discrete Fourier transform [29, 30], and the relation $\hat{\Gamma}(\mathbf{s})\hat{\Gamma}(\mathbf{t}) = \hat{\Gamma}(\mathbf{s} + \mathbf{t})$, the operators

$$\hat{\Pi}_{\mathbf{k}} = \sum_{\mathbf{s}} \frac{e^{-2\pi i \, \mathbf{k} \cdot \mathbf{s}}}{|\mathcal{S}|} \hat{\Gamma}(\mathbf{s}) \, , \, \mathbf{k} \in \mathbb{Z}_{\mathcal{S}} \, , \, \mathbf{k} \cdot \mathbf{s} = \sum_{i=0}^{r-1} \frac{k_i s_i}{n_i} \, , \, (6)$$

form a complete set of orthogonal projectors,

$$\hat{\Pi}_{\mathbf{k}} \hat{\Pi}_{\mathbf{k}'} = \delta_{\mathbf{k}\mathbf{k}'} \hat{\Pi}_{\mathbf{k}} \quad , \quad \sum_{\mathbf{k}} \hat{\Pi}_{\mathbf{k}} = \hat{\mathbb{1}} \quad . \quad (7)$$

Applying the projectors $\hat{\Pi}_{\mathbf{k}}$ to the basis functions, and orthonormalizing the resulting vectors, yields an orthonormal basis of symmetry-adapted orbitals $\{\tilde{\varphi}_{p\mathbf{k}_p}\}$. Here, and in the remainder of the present work, $\mathbf{k}_p \in \mathbb{Z}_{\mathcal{S}}$ denotes an irreducible representation or irrep, and p a group of $m_{\mathbf{k}_p}$ orbitals labelled by the irrep $\mathbf{k}_p$. The numbers $m_{\mathbf{k}_p}$ sum to M, and

$$\hat{\Pi}_{\mathbf{k}} |\tilde{\varphi}_{p\mathbf{k}_p}\rangle = \delta_{\mathbf{k}, \mathbf{k}_p} |\tilde{\varphi}_{p\mathbf{k}_p}\rangle \quad . \quad (8)$$

The number of irreps will be denoted $N_k = |\mathcal{S}|$. Since the orbitals $\tilde{\varphi}_{p\mathbf{k}_p}$ are eigenfunctions of the projectors $\hat{\Pi}_{\mathbf{k}}$, and the latter commute with the one- and two-body parts of the Hamiltonian, the matrix elements of $\hat{H}$ are sparse, as revealed by the expression

$$\hat{H} = E_0 + \sum_{\substack{\mathbf{k} \\ pq}} h_{pq}(\mathbf{k}) \hat{a}_{p\mathbf{k}}^\dagger \hat{a}_{q\mathbf{k}}$$

$$+ \sum_{\substack{\mathbf{k}_p \mathbf{k}_r \mathbf{k}_q \mathbf{k}_s \\ prqs}}^* \frac{(p\mathbf{k}_p, r\mathbf{k}_r | q\mathbf{k}_q, s\mathbf{k}_s)}{2} \hat{a}_{p\mathbf{k}_p}^\dagger \hat{a}_{q\mathbf{k}_q}^\dagger \hat{a}_{s\mathbf{k}_s} \hat{a}_{r\mathbf{k}_r} \quad (9)$$

where the $*$ over the summation denotes the constraint $\mathbf{k}_p + \mathbf{k}_q = \mathbf{k}_r + \mathbf{k}_s$ (with equality holding in the modular arithmetic of $\mathbb{Z}_{\mathcal{S}}$). (9) can be rewritten in terms of the transfer parameter $\mathbf{Q} = \mathbf{k}_p - \mathbf{k}_r = \mathbf{k}_s - \mathbf{k}_q$, leading to

$$\hat{H} = E_0 + \sum_{\substack{\mathbf{k} \\ pq}} h_{pq}(\mathbf{k}) \hat{a}_{p\mathbf{k}}^\dagger \hat{a}_{q\mathbf{k}}$$

$$+ \sum_{\substack{\mathbf{Q}\mathbf{k}_r \mathbf{k}_s \\ prqs}} \frac{(p\mathbf{k}_r + \mathbf{Q}, r\mathbf{k}_r | q\mathbf{k}_s - \mathbf{Q}, s\mathbf{k}_s)}{2} \quad (10)$$

$$\hat{a}_{p\mathbf{k}_r+\mathbf{Q}}^\dagger \hat{a}_{q\mathbf{k}_s-\mathbf{Q}}^\dagger \hat{a}_{s\mathbf{k}_s} \hat{a}_{r\mathbf{k}_r}$$

The structure of the Hamiltonian operator is illustrated in Figure 1. In the forthcoming sections, after providing a brief description of the AFQMC method, we will discuss in detail how the form of the Hamiltonian in (10) leads to savings in many of the operations in the method.

B.   The AFQMC method

The AFQMC method [14, 16, 17, 31] expresses the many-body ground state Ψ_0 of a Hamiltonian $\hat{H}$ through an imaginary time evolution,

$$|\Psi_0\rangle \propto \lim_{n \to \infty} e^{-n \, \Delta\tau (\hat{H} - E_0)} |\Phi_I\rangle \quad , \quad (11)$$

where $\Delta\tau$ (the time step) is chosen small and the initial state Φ_I, which should not be orthogonal to Ψ_0, is often a single Slater determinant. To sample the many-body propagator, we rewrite the Hamiltonian as

$$\hat{H} - E_0 = \hat{H}_1 - \frac{1}{2} \sum_\gamma \hat{v}_\gamma^2 \quad , \quad (12)$$

where $\hat{H}_1$, $\hat{v}_\gamma$ are one-body operators. Then, using a Hubbard-Stratonovich transformation [32, 33], the short-imaginary-time propagator is

$$e^{-\Delta\tau(\hat{H} - E_0)} = \int d\mathbf{x} \, p(\mathbf{x}) \, \hat{B}(\mathbf{x}), \quad (13)$$

where

$$\hat{B}(\mathbf{x}) = e^{-\frac{\Delta\tau}{2} \hat{H}_1} e^{\sqrt{\Delta\tau} \sum_\gamma x_\gamma \hat{v}_\gamma} e^{-\frac{\Delta\tau}{2} \hat{H}_1} \quad (14)$$

is a one-body propagator that is a function of the multi-dimensional vector $\mathbf{x}$, and $p(\mathbf{x})$ is the standard normal probability distribution. AFQMC thus represents the many-body wave function as a superposition of non-orthogonal Slater determinants,

$$|\Phi_n\rangle = e^{-n \, \Delta\tau(\hat{H} - E_0)} |\Phi_I\rangle = \int \prod_{l=0}^{n-1} d\mathbf{x}_l \, p(\mathbf{x}_l) \hat{B}(\mathbf{x}_l) |\Phi_I\rangle .$$

$$(15)$$

The ground-state expectation value of $\hat{H}$ is obtained as

$$\frac{\langle \Psi_T | \hat{H} | \Phi_n \rangle}{\langle \Psi_T | \Phi_n \rangle} =$$

$$\frac{\int \prod_{l=0}^{n-1} d\mathbf{x}_l \, p(\mathbf{x}_l) \langle \Psi_T | \hat{H} | \prod_{l=0}^{n-1} \hat{B}(\mathbf{x}_l) | \Phi_I \rangle}{\int \prod_{l=0}^{n-1} d\mathbf{x}_l \, p(\mathbf{x}_l) \langle \Psi_T | \prod_{l=0}^{n-1} \hat{B}(\mathbf{x}_l) | \Phi_I \rangle} = \quad (16)$$

$$\frac{\int d\mathbf{X} \, p(\mathbf{X}) \, W(\mathbf{X}) \, \mathcal{E}_{loc}(\Phi_n(\mathbf{X}))}{\int d\mathbf{X} \, p(\mathbf{X}) \, W(\mathbf{X})} \quad ,$$

where Ψ_T is a second many-body state, called the trial wavefunction. In Eq. (16), the overlap and local energy,

$$W(\mathbf{X}) = \langle \Psi_T | \prod_{l=0}^{n-1} \hat{B}(\mathbf{x}_l) | \Phi_I \rangle \equiv \langle \Psi_T | \Phi_n(\mathbf{X}) \rangle \quad ,$$

$$\mathcal{E}_{loc}(\Phi_n(\mathbf{X})) = \frac{\langle \Psi_T | \hat{H} | \Phi_n(\mathbf{X}) \rangle}{\langle \Psi_T | \Phi_n(\mathbf{X}) \rangle} \quad ,$$
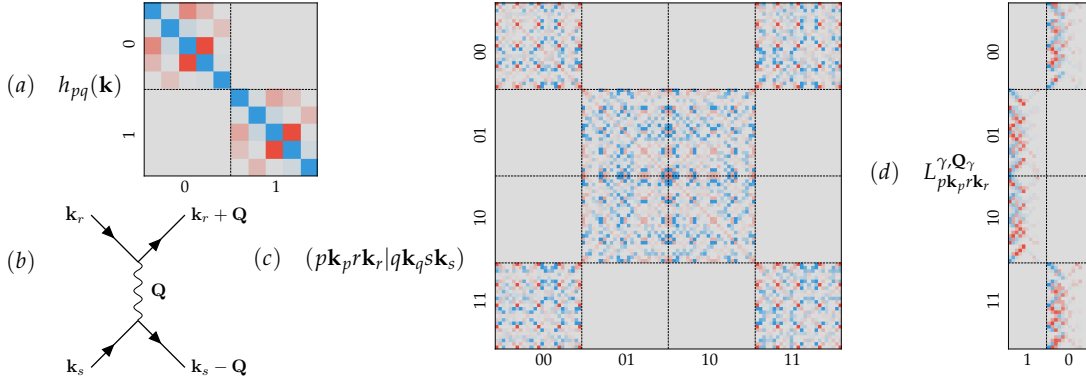
$$(17)$$

FIG. 1. (color online) Illustrative matrix elements of the Hamiltonian for a chain of 10 H atoms spaced by a distance of $R = 1\text{Å}$, in the STO-6G basis. To account for reflection symmetry across a plane perpendicular to the chain we construct a basis of orthonormal symmetry-adapted orbitals (even, odd denoted 0, 1 respectively). (a) The one-body part of the Hamiltonian is block-diagonal. (b) Conservation of $\mathbf{k}_r + \mathbf{k}_s$ (in this case parity) can be depicted in a two-vertex Feynman diagram. (c) Sparsity in the electron repulsion integral (ERI), from the condition $\mathbf{k}_r + \mathbf{k}_s = \mathbf{k}_p + \mathbf{k}_q$ (where sum is performed modulo 2). (d) Cholesky decomposition of the ERI: $L^{\gamma \mathbf{Q}_\gamma}_{\mathbf{k}_p p, \mathbf{k}_r r} \neq 0$ only for $\mathbf{Q}_\gamma = \mathbf{k}_p - \mathbf{k}_r$. Matrix elements are rescaled to enhance visibility, warm (cold) colors denote positive (negative) values.

are defined on a path $\mathbf{X} = (\mathbf{x}_{n-1} \ldots \mathbf{x}_0)$ of auxiliary fields at each time slice up to $n - 1$. The expectation value is computed over a collection of Monte Carlo (MC) samples (labeled by i) as

$$\frac{\langle \Psi_T | \hat{H} | \Psi_0 \rangle}{\langle \Psi_T | \Psi_0 \rangle} \simeq \frac{\sum_i W_i \, \mathcal{E}_{loc}(\Phi_i)}{\sum_i W_i} . \tag{18}$$

and the stochastically sampled determinants Φ_i are called walkers in the AFQMC literature.

Because the propagator $\hat{B}(\mathbf{x})$ contains stochastically fluctuating fields, the MC sampling will lead to complex overlaps W_i, which causes the variance of this estimator to grow exponentially with the number of time-steps n. This phase problem can be controlled by an approximate gauge condition known as the phaseless approximation [14, 16, 17, 31], which we summarize below:

1. MEAN-FIELD BACKGROUND SUBTRACTION: the expectation values $\langle \hat{v}_\gamma \rangle_T = \langle \Psi_T | \hat{v}_\gamma | \Psi_T \rangle$ are computed and the Hamiltonian is rewritten as

$$\hat{H} - E_0 = \hat{H}'_1 - \frac{1}{2} \sum_\gamma (\hat{v}_\gamma - \langle \hat{v}_\gamma \rangle_T)^2 \quad , \tag{19}$$

2. IMPORTANCE SAMPLING TRANSFORMATION: the Hubbard-Stratonovich is defined up to a shift $\mathbf{x} \to \mathbf{x} - \overline{\mathbf{x}}$, $\overline{\mathbf{x}} \in \mathbb{C}$, and this additional freedom is exploited to rewrite the estimator (16) with the replacements

$$\hat{B}(\mathbf{x}) \to \hat{B}'(\mathbf{x} - \overline{\mathbf{x}}) = e^{-\frac{\Delta\tau}{2} \hat{H}'_1} e^{\sqrt{\Delta\tau} \sum_\gamma (x_\gamma - \overline{x}_\gamma) \hat{v}'_\gamma} e^{-\frac{\Delta\tau}{2} \hat{H}'_1} ,$$

$$\prod_{l=0}^{n-1} \hat{B}(\mathbf{x}_l) | \Phi_I \rangle \to \prod_{l=0}^{n-1} \hat{B}'(\mathbf{x}_l - \overline{\mathbf{x}}_l) | \Phi_I \rangle \equiv | \Phi'_n(\mathbf{X}, \overline{\mathbf{X}}) \rangle ,$$

$$W'(\mathbf{X}) \to \prod_{l=0}^{n-1} I\left(\mathbf{x}_l, \overline{\mathbf{x}}_l; \Phi'_l(\mathbf{X}, \overline{\mathbf{X}})\right) ,$$

$$I\left(\mathbf{x}, \overline{\mathbf{x}}; \Phi\right) = \frac{p(\mathbf{x} - \overline{\mathbf{x}})}{p(\mathbf{x})} \frac{\langle \Psi_T | \hat{B}'(\mathbf{x}_l - \overline{\mathbf{x}}_l) | \Phi \rangle}{\langle \Psi_T | \Phi \rangle} , \tag{20}$$

where $\hat{v}'_\gamma = \hat{v}_\gamma - \langle \hat{v}_\gamma \rangle_T$. One makes the choice

$$\overline{\mathbf{x}}_\gamma = -\sqrt{\Delta\tau} \frac{\langle \Psi_T | \hat{v}'_\gamma | \Phi \rangle}{\langle \Psi_T | \Phi \rangle} \equiv -\sqrt{\Delta\tau} \langle \hat{v}'_\gamma \rangle \tag{21}$$

to minimize fluctuations in the importance function $I(\mathbf{x}, \overline{\mathbf{x}}; \Phi)$ to leading order in $\Delta\tau$.

3. Real local energy and cosine approximations: the importance function is approximated as

$$I\left(\mathbf{x}, \overline{\mathbf{x}}; \Phi\right) \simeq e^{-\Delta\tau \, \mathrm{Re}\, (\mathcal{E}_{loc}(\Phi) - E_0)} \, \max\left(0, \cos(\Delta\theta)\right) \quad ,$$

$$\Delta\theta = \mathrm{Arg} \frac{\langle \Psi_T | \hat{B}'(\mathbf{x} - \overline{\mathbf{x}}) | \Phi \rangle}{\langle \Psi_T | \Phi \rangle} \quad . \tag{22}$$

Steps 1, 2 are simply re-parametrizations which reduce fluctuations in the estimators of physical properties when $\overline{\mathbf{x}}_\gamma$ is real. When it is complex, these transformations ensure that the gauge variation is minimized, enabling the sign problem to be removed in step 3. The bias resulting from the approximations in step 3 can be reduced by improving the trial wavefunction. AFQMC has been

successfully applied to multiple lattice models of correlated electrons [34–36] and real materials [37–39]. There are many additional algorithmic improvements and extensions, for example to compute properties [40–42], and to improve the efficiency of the method [17, 43].

III. METHOD

We now illustrate how to account for Hamiltonian symmetries in the above procedure. Additional implementation details appear in the Appendices. In what follows, we consider a symmetry group composed of N_k Abelian symmetries, with irreps labelled by $\mathbf{k}$. We use the symbols M, N, N_γ to denote the total number of basis functions, particles and auxiliary fields respectively. Correspondingly, we use $m_\mathbf{k}$, $n_\mathbf{k}$ and $n_{\gamma,\mathbf{k}}$ to denote the number of basis functions, particles and auxiliary fields labelled by the irrep $\mathbf{k}$, and m, n, n_γ to denote the average numbers of basis functions, particles and auxiliary fields per irrep, $m = \sum_\mathbf{k} m_\mathbf{k}/N_k$ etc. Indices $prqs$, ij, γ run over basis functions, particles and auxiliary fields labelled by

a specific irrep $\mathbf{k}$, respectively.

A. Hamiltonian representation

As expressed in (12), in AFQMC we must express the two-body part of the Hamiltonian as a sum of squares of one-body operators. To achieve this, one commonly relies on a density fitting (DF) [44, 45] or Cholesky decomposition (CD) [46–49] of the electron repulsion integrals, $(pr|qs) \simeq \sum_{\gamma=1}^{N_\gamma} L_{pr}^\gamma L_{qs}^\gamma$ where N_γ is the number of components. As detailed in Appendix A 2, in the presence of symmetries, such a decomposition becomes

$$\frac{(p\mathbf{k}_r+\mathbf{Q}, r\mathbf{k}_r|q\mathbf{k}_s-\mathbf{Q}, s\mathbf{k}_s)}{2} = \sum_\gamma L_{p\mathbf{k}_r+\mathbf{Q}, r\mathbf{k}_r}^{\gamma,\mathbf{Q}} L_{q\mathbf{k}_s-\mathbf{Q}, s\mathbf{k}_s}^{\gamma,-\mathbf{Q}} ,$$
(23)

where, as illustrated in Figure 1, components γ are labelled by irreps $\mathbf{Q}$, $-\mathbf{Q}$, the number of which $n_{\gamma,\mathbf{Q}}$ sums to N_γ. Then (as detailed in Appendix B) we interchange the creation and destruction operators in (10) and use (23) to rewrite the Hamiltonian as a sum of squares,

$$\hat{H} - E_0 = \sum_{\substack{\mathbf{k} \\ pq}} \tilde{h}_{pq}(\mathbf{k})\hat{a}_{p\mathbf{k}}^\dagger \hat{a}_{q\mathbf{k}} - \frac{1}{2} \sum_{\gamma\mathbf{Q}} \left[\left(\frac{i\hat{L}_{\gamma,\mathbf{Q}} + i\hat{L}_{\gamma,-\mathbf{Q}}}{\sqrt{2}} \right)^2 + \left(\frac{\hat{L}_{\gamma,\mathbf{Q}} - \hat{L}_{\gamma,-\mathbf{Q}}}{\sqrt{2}} \right)^2 \right] , \tag{24}$$

where

$$\hat{L}_{\gamma,\mathbf{Q}} = \sum_{\substack{\mathbf{k}_r \\ rp}} L_{p\mathbf{k}_r+\mathbf{Q}, r\mathbf{k}_r}^{\gamma,\mathbf{Q}} \hat{a}_{p\mathbf{k}_r+\mathbf{Q}}^\dagger \hat{a}_{r\mathbf{k}_r} . \tag{25}$$

The total number of auxiliary fields is thus $2N_\gamma$, where the correspondence with the label γ in (12) is $\gamma \to (\gamma,\mathbf{Q},1)$, $(\gamma,\mathbf{Q},2)$ and the auxiliary field operators are $\hat{v}_{\gamma,\mathbf{Q},1} = (i\hat{L}_{\gamma,\mathbf{Q}} + i\hat{L}_{\gamma,-\mathbf{Q}})/\sqrt{2}$ and $\hat{v}_{\gamma,\mathbf{Q},2} = (\hat{L}_{\gamma,\mathbf{Q}} - \hat{L}_{\gamma,-\mathbf{Q}})/\sqrt{2}$ respectively. A simple technique to reduce the number of auxiliary fields to N_γ is described in Appendix B 3.

Importantly, the correction to the one-body part of the Hamiltonian resulting from the interchange of creation and destruction operators in (10) does not mix orbitals labeled by different irreps (i.e. it is block-diagonal). Additional details are given in Appendix B 1.

It is clear that the Hamiltonian integrals, such as $(p\mathbf{k}_r+\mathbf{Q}, r\mathbf{k}_r|q\mathbf{k}_s-\mathbf{Q}, s\mathbf{k}_s)$, require $1/N_k$ less storage than without symmetry. The coefficients defining $\hat{L}_{\gamma,\mathbf{Q}}$ also show a $1/N_k$ reduction in storage compared to without symmetry.

B. Mean-field wavefunction and background subtraction

We assume that the trial wavefunction is a single determinant. If the single determinant wavefunction transforms as an irrep of $\mathcal{S}$, then its orbitals $\psi_{i\mathbf{k}_i}$ can also be labelled by irreps, thus

$$|\Psi_T\rangle = \prod_{i\mathbf{k}_i} \hat{a}_{\psi_{i\mathbf{k}_i}}^\dagger |\emptyset\rangle ,$$
$$\hat{a}_{\psi_{i\mathbf{k}_i}}^\dagger = \sum_r \left(\Psi_T(\mathbf{k}_i) \right)_{ri} \hat{a}_{r\mathbf{k}_r}^\dagger , \tag{26}$$

where the numbers $n_\mathbf{k}$ of particles in each orbital irrep satisfy $\sum_\mathbf{k} n_\mathbf{k} = N$ and the coefficient matrix $\Psi_T(\mathbf{k}_i)$ is blocked by symmetry. In contrast, a generic Slater determinant (such as the walkers in an AFQMC calculation) is parametrized by a dense $M \times N$ matrix $\Phi_{r\mathbf{k}_r,i\mathbf{k}_i}$. An important property of (26) is that the one-body density matrix

$$\rho_{r\mathbf{k}_r, p\mathbf{k}_p} = \langle \Psi_T | \hat{a}_{p\mathbf{k}_p}^\dagger \hat{a}_{r\mathbf{k}_r} | \Psi_T \rangle$$
$$= \delta_{\mathbf{k}_p \mathbf{k}_r} \left[\Psi_T(\mathbf{k}_r)\Psi_T^\dagger(\mathbf{k}_r) \right]_{rp} \tag{27}$$

is also block-diagonal. The mean-field expectation values of the operators $\hat{L}_{\gamma,\mathbf{Q}}$ thus read

$$\langle \Psi_T | \hat{L}_{\gamma,\mathbf{Q}} | \Psi_T \rangle = \delta_{\mathbf{Q},\mathbf{0}} \, \ell_\gamma \ . \tag{28}$$

Defining the operators

$$\hat{L}'_{\gamma,\mathbf{Q}} = \hat{L}_{\gamma,\mathbf{Q}} - \frac{\delta_{\mathbf{Q},\mathbf{0}} \, \ell_\gamma}{N} \, \hat{N} \quad , \tag{29}$$

which by construction have zero average over Ψ_T, we can obtain operators with the mean-field background subtracted, as in (19) and detailed in Appendix B 2,

$$\hat{v}'_{\gamma\mathbf{Q},1} = \frac{i\hat{L}'_{\gamma,\mathbf{Q}} + i\hat{L}'_{\gamma,-\mathbf{Q}}}{\sqrt{2}}$$
$$\hat{v}'_{\gamma\mathbf{Q},2} = \frac{\hat{L}'_{\gamma,\mathbf{Q}} - \hat{L}'_{\gamma,-\mathbf{Q}}}{\sqrt{2}} \tag{30}$$

In this step, the trial wavefunction requires storing $\sum_{\mathbf{k}} m_{\mathbf{k}} n_{\mathbf{k}} \simeq mnN_k$ coefficients, a reduction of $1/N_k$ compared to without symmetry. Similarly, the block structure of the trial wavefunction and density matrix means that computing the mean-field density matrix and subsequent background term also involves a $1/N_k$ reduction in the number of operations.

C. Overlap calculation

The overlap matrix between the trial wavefunction and a walker

$$|\Phi\rangle = \prod_{j\mathbf{k}_j} \hat{a}^\dagger_{\Phi_{j\mathbf{k}_j}} |\emptyset\rangle \tag{31}$$

is $\langle \Psi_T | \Phi \rangle = \det(\Omega)$, with

$$(\Omega)_{i\mathbf{k}_i,j\mathbf{k}_j} = \sum_r \left(\Psi_T(\mathbf{k}_i) \right)^\dagger_{ir} \Phi_{r\mathbf{k}_i,j\mathbf{k}_j} \quad . \tag{32}$$

Due to the symmetry block structure of Ψ_T, computing Ω requires $\mathcal{O}(mN^2)$ operations, even though Ω is in general dense. Compared to the corresponding cost of $\mathcal{O}(MN^2)$ in a calculation that does not exploit symmetry, this is more efficient by a factor of $1/N_k$.

D. Force bias calculation

Using symmetry, the force bias calculation involves the quantities $\langle \hat{v}'_\gamma \rangle$. These are easily related to

$$\langle \hat{L}_{\gamma,\mathbf{Q}} \rangle \equiv \sum_{\substack{\mathbf{k}_r \\ pr}} L^{\gamma,\mathbf{Q}}_{p\mathbf{k}_p,r\mathbf{k}_r} \frac{\langle \Psi_T | \hat{a}^\dagger_{p\mathbf{k}_p} \hat{a}_{r\mathbf{k}_r} | \Phi \rangle}{\langle \Psi_T | \Phi \rangle} \quad , \tag{33}$$

with $\mathbf{Q} = \mathbf{k}_p - \mathbf{k}_r$, which are calculated as

$$\langle \hat{L}_{\gamma,\mathbf{Q}} \rangle = \sum_{\substack{\mathbf{k}_r \\ ir}} \mathcal{L}^{\gamma,\mathbf{Q}}_{i\mathbf{k}_p,r\mathbf{k}_r} \Theta_{r\mathbf{k}_r,i\mathbf{k}_p} \quad ,$$
$$\mathcal{L}^{\gamma,\mathbf{Q}}_{i\mathbf{k}_p,r\mathbf{k}_r} = \sum_p \left(\Psi_T(\mathbf{k}_p) \right)^\dagger_{ip} L^{\gamma,\mathbf{Q}}_{p\mathbf{k}_p,r\mathbf{k}_r} \quad , \tag{34}$$

where $\mathbf{Q} = \mathbf{k}_p - \mathbf{k}_r$ and $\Theta = \Omega^{-1}\Phi$. $\mathcal{L}$ can be precomputed, storing $mnn_\gamma N_k^2$ complex numbers. The computational cost to obtain the force bias with precomputation is $\mathcal{O}(mnn_\gamma N_k^2)$. Compared with the cost of a calculation that does not exploit symmetry (MNN_γ operations) this is more efficient by a factor $1/N_k$. Note, however, that while we can use symmetry when generating the matrix Ω, as discussed in Section III C, the cost of computing its determinant and its inverse is not reduced by symmetry, because it is in general dense. There is thus only a partial gain due to symmetry for the force bias calculation.

E. Walker propagation

With symmetry, the small-imaginary time propagator in (13) takes the form

$$e^{-\Delta\tau(\hat{H}-E_0)} = e^{-\frac{\Delta\tau}{2}\hat{H}'_1} \int d\mathbf{x} \, e^{\hat{A}(\mathbf{x})} e^{-\frac{\Delta\tau}{2}\hat{H}'_1} \quad , \tag{35}$$

for operators $\hat{A}(\mathbf{x})$, defined as a linear combination of $x_{\mathbf{Q}\gamma 1}\hat{v}'_{\gamma,\mathbf{Q},1}$, $x_{\mathbf{Q}\gamma 2}\hat{v}'_{\gamma,\mathbf{Q},2}$, as derived in Appendix B 3. Applying the exponential of $\hat{H}'_1$ to a (walker) Slater determinant can be carried out efficiently. In fact, since $\hat{H}'_1$ is symmetric and thus does not mix irreps, it has the form $\hat{H}'_1 = \sum_{\mathbf{k}pq} h'_{pq}(\mathbf{k}) \, \hat{a}^\dagger_{p\mathbf{k}} \hat{a}_{q\mathbf{k}}$. Thus if the walker $|\Phi\rangle$ is parametrized by the matrix $\Phi_{p\mathbf{k}_p,i\mathbf{k}_i}$, its image $|\Phi'\rangle = e^{-\frac{\Delta\tau}{2}\hat{H}'_1} |\Phi\rangle$ from the one-body propagator is parametrized by the matrix

$$(\Phi')_{p\mathbf{k}_p,i\mathbf{k}_i} = \sum_q \left(e^{-\frac{\Delta\tau}{2}h'(\mathbf{k}_p)} \right)_{pq} (\Phi')_{q\mathbf{k}_p,i\mathbf{k}_i} \quad . \tag{36}$$

This can be computed using $\mathcal{O}(m^2 N N_k)$ operations, as compared to $\mathcal{O}(M^2 N)$ operations in a calculation that does not use symmetry. To propagate the interacting part of $\hat{H}$, one possible strategy is to construct the matrix $\mathcal{A}_{p\mathbf{k}_p,r\mathbf{k}_r}$ associated with the operator $\hat{A}(\mathbf{x})$ and then apply $e^{\mathcal{A}}$ to Φ. The cost to construct $\mathcal{A}$ is $\mathcal{O}(m^2 n_\gamma N_k^2)$ (it is a linear combination of block sparse matrices), a reduction of $1/N_k$ compared to without symmetry. However, since in general $\mathcal{A}$ lacks any sparsity properties, the cost of applying its exponential to Φ requires $\mathcal{O}(M^2 N)$ operations. Note that, in principle, sparsity could be exploited by applying individual terms of $e^{\hat{A}}$, such as $e^{\sqrt{\Delta\tau}ix_{\mathbf{Q}\gamma 1}\hat{v}'_{\gamma,\mathbf{Q},1}}$, where such an exponential is further expanded as a power series with each term transforming as

an irrep and corresponding to sparse matrix multiplication onto Φ. However, this is only a savings for symmetry groups where the number of irreps far exceeds the number of terms in the power series. We have not observed savings with this second strategy in this work. Thus we only report calculations where we apply the full $\mathcal{A}$ matrix, with only a partial (i.e. limited to the generation of $\mathcal{A}$) reduction in cost in this step from symmetry.

F. Local energy calculation

For the one-body part of the local energy, the form of the estimator and the speedup over implementations without symmetry are very similar to the case of the force bias. Indeed, an analogous calculation leads to the expressions

$$
\begin{aligned}
\mathcal{E}_{loc,1}(\Phi) &= \sum_{\substack{\mathbf{k}_i \\ ir}} \mathcal{K}_{ir}(\mathbf{k}_i)\Theta_{r\mathbf{k}_i,i\mathbf{k}_i}\ , \\
\mathcal{K}_{ir}(\mathbf{k}) &= \sum_p \left(\Psi_T(\mathbf{k})\right)^\dagger_{ip} h_{pr}(\mathbf{k})
\end{aligned}
\tag{37}
$$

For the considerably more expensive two-body part, we use the generalized Wick's theorem [50, 51] to obtain

$$
\mathcal{E}_{loc,2}(\Phi) = \sum_{\mathbf{Q}\gamma} \sum_{\substack{\mathbf{k}_r \mathbf{k}_s \\ ij}} f^\gamma_{i\mathbf{k}_p,i\mathbf{k}_r} f^\gamma_{j\mathbf{k}_q,j\mathbf{k}_s} - f^\gamma_{i\mathbf{k}_p,j\mathbf{k}_q} f^\gamma_{j\mathbf{k}_q,i\mathbf{k}_p}
\tag{38}
$$

where ij are associated with particles labelled by the irreps $\mathbf{k}_p = \mathbf{k}_r + \mathbf{Q}$, $\mathbf{k}_q = \mathbf{k}_s - \mathbf{Q}$ respectively, and the tensor f is defined as

$$
f^\gamma_{i\mathbf{k}_p,j\mathbf{k}_q} = \sum_r \mathcal{L}^\gamma_{i\mathbf{k}_p,r\mathbf{k}_r} \Theta_{r\mathbf{k}_r,j\mathbf{k}_q}\quad .
\tag{39}
$$

As seen, the cost of the procedure is $\mathcal{O}(mn^2 n_\gamma N_k^3)$ operations to generate the tensor f, and $\mathcal{O}(n^2 n_\gamma N_k^3)$ to perform the final contraction. Compared with a calculation without symmetry, this is more efficient by a factor of $1/N_k$.

G. Summary

The acceleration achieved in AFQMC due to the use of symmetries is summarized in Table I. Most computational steps are accelerated by a factor of $1/N_k$, and storage is reduced by $1/N_k$ as well. In a standard mean-field calculation, symmetries lead to an acceleration by a factor of $1/N_k^2$, due to symmetries in both the Hamiltonian as well as the wavefunction. In AFQMC, the acceleration is limited to $1/N_k$ because the walkers do not transform as irreps of $\mathcal{S}$, as individual components of the Hubbard-Stratonovich such as $\hat{L}_{\gamma,\mathbf{Q}}$ all transform as different irreps of $\mathcal{S}$.

IV. RESULTS

We now present some illustrative calculations using symmetry in AFQMC calculations for a molecule and for crystalline systems. Restricted Hartree-Fock (RHF), density functional theory (DFT), Møller-Plesset perturbation theory (MP2) and coupled-cluster with singles and doubles (CCSD) calculations were performed with the PySCF package [8].

1. MOLECULAR CALCULATIONS: we perform all-electron calculations using the standard cc-pVTZ basis [52, 53] from quantum chemistry. We obtain the auxiliary-field representation by a Cholesky decomposition, and use the RHF state as a trial wavefunction.

2. CRYSTALLINE CALCULATIONS: we replace core electrons by norm-conserving GTH Padé pseudopotentials [7, 54, 55]. We compute Hamiltonian matrix elements with the PySCF program [8] using the GTH series of Gaussian bases [56]. We use Gaussian density fitting to treat the electron-electron interaction and to obtain the auxiliary-field representation [21]. We report RHF energies using the leading finite size correction for the $\mathbf{G} = 0$ contribution to the Hartree-Fock exchange (`exxdiv=ewald`) and obtain total energies from other methods by adding this RHF energy to the respective correlation energies, with integrals computed omitting the $\mathbf{G} = 0$ term (`exxdiv=None`) [7, 8]. We use the RHF state as a trial wavefunction.

A. Molecular systems and point group symmetry

As a simple test-case, we first consider a molecular system, SF_6, where we use the reflection group symmetry. The reflection group is isomorphic to $\mathbb{Z}_2^3$, where 3 is the number of reflection planes, giving 8 irreps in the group.

In Fig. 2 we show the equation of state $E(R)$ of the molecule (where R is the S-F bond length) using AFQMC, DFT with the B3LYP functional, RHF and CCSD. As can be seen, the AFQMC calculations performed with and without reflection symmetry (red circles and dark red crosses in Fig. 2) yield identical results to within statistical error. CCSD and AFQMC yield potential energy surfaces in reasonable agreement with each other.

B. Crystalline solids

The computational saving from symmetries is especially important in systems with a large symmetry group, and crystalline solids form one such example. Consider a crystal with a primitive cell with lattice vectors $\mathbf{a}_0$, $\mathbf{a}_1$, $\mathbf{a}_2$. We use translational-symmetry-adapted (crystalline)

operation	without symmetry	with symmetry	savings
storage of integrals	$M^2 + M^2 N_\gamma + MN$	$m^2 N_k + m^2 n_\gamma N_k^2 + mn N_k$	N_k^{-1}
no. of auxiliary fields	N_γ	$n_\gamma N_k$	none
force bias calculation	MNN_γ	$mnn_\gamma N_k$	N_k^{-1}
overlap, Θ matrix	$MN^2 + N^3 + M^2 N$	$mN^2 + N^3 + M^2 N$	N_k^{-1} (partial)
propagation (kinetic)	$M^2 N$	$m^2 N N_k$	N_k^{-1}
propagation (potential)	$M^2 N_\gamma + M^2 N$	$m^2 n_\gamma N_k + M^2 N$	N_k^{-1} (partial)
local energy calculation	$NM + MN^2 N_\gamma$	$mn N_k + mn^2 n_\gamma N_k^3$	N_k^{-1}

TABLE I. Comparison of the computational cost of the main operations in an AFQMC calculation, without (left) and with the use of symmetry (right). In most cases, a cost reduction by a factor of N_k^{-1} is seen. The three terms under "storage of integrals" refer to the one- and two-body parts of $\hat{H}$ and the trial wavefunction respectively. The two terms under "overlap, Θ matrix" refer to the construction and inversion of the overlap matrix and construction of the Θ matrix respectively. The two terms under "propagation (potential)" refer to construction and application of the $\mathcal{A}$ matrix. The two terms under "local energy calculation" refer to one- and two-body parts of the local energy.
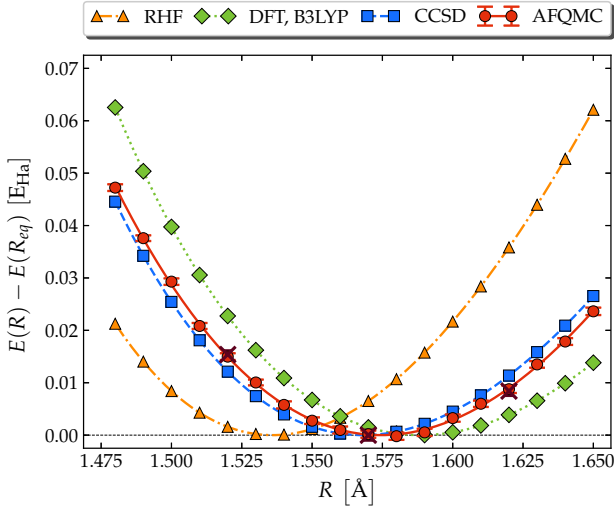

FIG. 2. Energy as function of bondlength for SF_6 for RHF, DFT-B3LYP, CCSD and AFQMC with and without reflection symmetry (red circles, dark red crosses) in the cc-pVTZ basis. Energies are shown relative to the minimum value $E(R_{eq})$.

Gaussian atomic orbitals [7] (AOs) as a symmetry basis. Starting from a set of Gaussian AOs in the primitive cell φ_μ, these can be written as

$$|\tilde{\varphi}_{\mu\mathbf{k}}\rangle = \sum_{\mathbf{i}} \frac{e^{-2\pi i\, \mathbf{i}\cdot\mathbf{k}}}{\sqrt{N_k}} |\varphi_{\mu\mathbf{i}}\rangle \quad , \tag{40}$$

where $\mathbf{i}$ is an integer vector (i_0, i_1, i_2) denoting φ_μ translated from the primitive cell by lattice vector $\sum_{r=0}^{2} i_r \mathbf{a}_r$, and $\mathbf{k}$ has the form $\sum_{r=0}^{2} \frac{k_r}{N_r} \mathbf{b}_r$, where k_r is an integer vector with $0 \le k_r < N_r$ and $\mathbf{b}_r$ are the reciprocal lattice vectors. This choice of k_r is equivalent to sampling the Brillouin zone with a mesh of $N_0 \times N_1 \times N_2$ wavevectors including the Γ point (origin). Note the above basis representation spans the same Hilbert space as a $N_0 \times N_1 \times N_2$ supercell calculation with (Γ point) periodic boundary conditions [18].

The Hamiltonian symmetries are the lattice translations, corresponding to integer multiples $\sum_{r=0}^{2} s_r \mathbf{a}_r$ of the $\mathbf{a}_0$, $\mathbf{a}_1$, $\mathbf{a}_2$ vectors. Under such translations, the basis transforms as

$$\hat{\Gamma}(\mathbf{s}) |\tilde{\varphi}_{\mu\mathbf{k}}\rangle = e^{2\pi i \sum_r \frac{s_r k_r}{N_r}} |\tilde{\varphi}_{\mu\mathbf{k}}\rangle \tag{41}$$

thus, the translation group is isomorphic to $\mathbb{Z}_{N_0} \times \mathbb{Z}_{N_1} \times \mathbb{Z}_{N_2}$.

To demonstrate the symmetry-adapted AFQMC using the lattice translation group we first compute the equilibrium lattice constants of C diamond and Si FCC in Figure 3, using a $2\times2\times2$ k-point mesh, at the GTH-DZV level. Here we find that AFQMC is in good agreement with CCSD using the same k-point mesh, and significantly improves on RHF and MP2. This trend can be seen in the potential energy surfaces in Figure 3, as well as in the corresponding equilibrium lattice constants.

Using translational symmetry, we can further consider larger symmetry groups in order to extrapolate to the thermodynamic limit (TDL). Note that increasing the size of the translational symmetry group yields the same result as a calculation with increased supercell size, but with much reduced cost.

We illustrate the extrapolation of results to the thermodynamic limit in Figure 4, using C diamond as a test system. RHF and correlation energies were computed for $2\times2\times2$, $2\times2\times3$, $3\times3\times3$, $3\times3\times4$, $4\times4\times3$ and $4\times4\times4$ meshes of k-points, using the GTH-DZV basis. In the upper panel of Figure 4 we show the equation of state $E_{TDL}(R)$ extrapolated to the thermodynamic limit (with the minimum value $E_{TDL}(R_{eq})$ subtracted) from RHF, MP2 and AFQMC.

We extrapolate RHF total energies and AFQMC, MP2 correlation energies (per cell) to the TDL using power-law Ansatz $E(N_k) = \alpha + \beta N_k^\mu$, with $\mu = -1$ for RHF and AFQMC [57] and $\mu = -\frac{1}{3}$ for MP2 [7]. Extrapolation of RHF (correlation) energies is carried out using data for all but the smallest two (the smallest) k-point meshes. In the lower panel of Figure 4, we illustrate the extrapolation of MP2 (left) and AFQMC (right) correla-
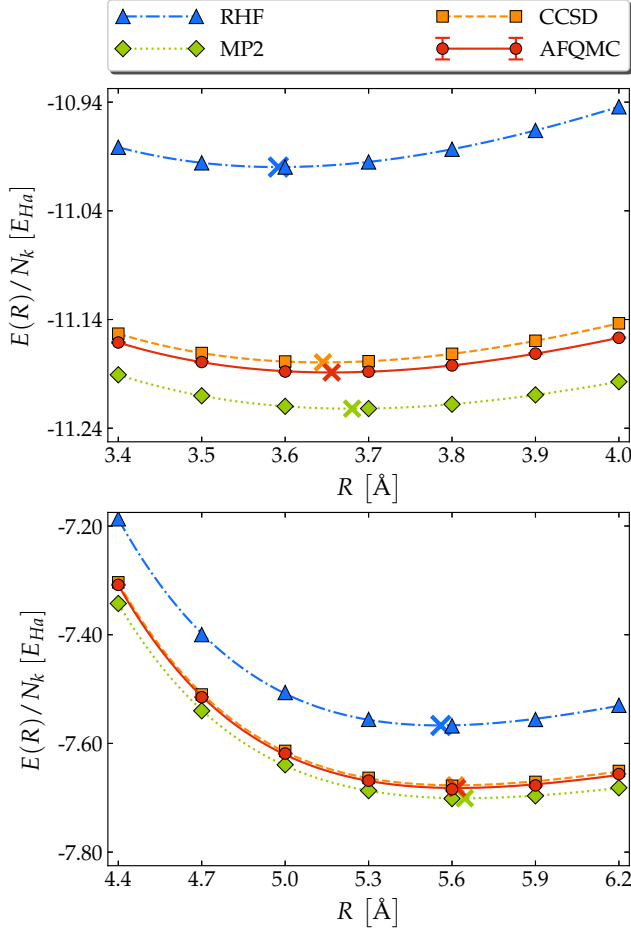
FIG. 3. Equation of state of C diamond (top) and Si FCC (bottom), using a 2×2×2 k-point mesh and the GTH-DZV basis and GTH Padé pseudopotential, from RHF, MP2, CCSD, AFQMC (blue triangles, green diamonds, orange squares, red circles). Crosses denote equilibrium bondlengths.
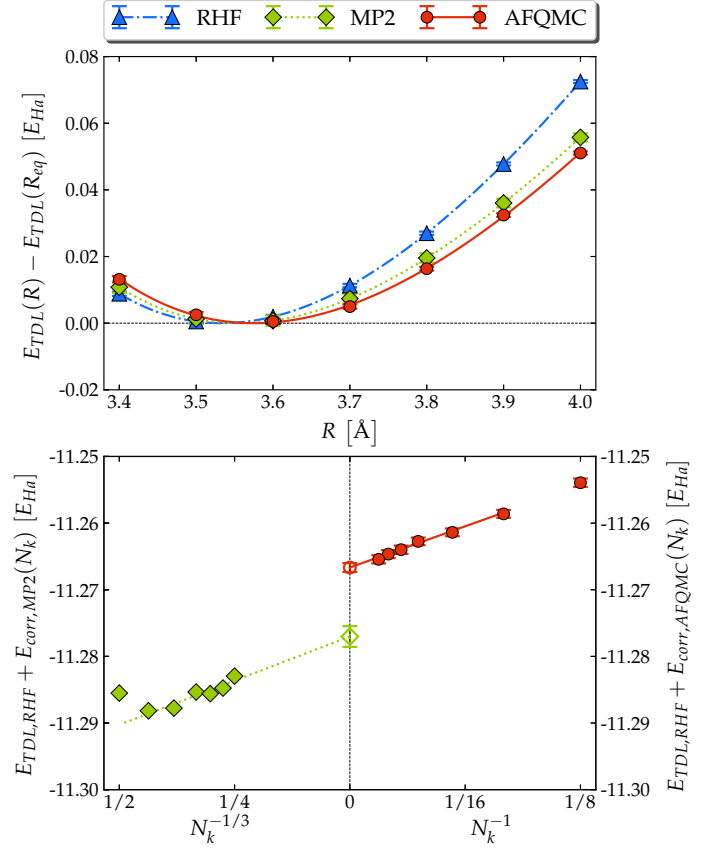

FIG. 4. Top: Equation of state of C diamond from RHF, MP2 and AFQMC (blue triangles, green diamonds, red circles) extrapolated to the thermodynamic limit, in the GTH-DZV basis, using the GTH-Padé pseudopotential. Bottom: detail of the thermodynamic limit extrapolation for the MP2 (left) and AFQMC (right) correlation energy. Extrapolated quantities are shown with empty symbols.

tion energies at the representative bondlength $R = 3.6$ Å.

Fitting the TDL curves to the Morse potential Ansatz $E(R) = E_0 + \Delta E \left(1 - e^{-\alpha(R-R_{eq})}\right)^2$ gives an equilibrium bondlength of $R_{eq,AFQMC} = 3.575(1)$ Å. For the 2×2×2 supercell, the same procedure yields $R_{eq,AFQMC} = 3.657(1)$ Å, thus TDL extrapolation significantly shortens the AFQMC equilibrium bondlength. For reference, the experimental bondlength is $R = 3.553$ Å, corrected for zero-point vibrational effects [58]; for a more faithful comparison, a larger basis set should be used [25].

In Figure 5 we carry out a similar calculation for 2D hexagonal boron nitride. RHF energies and AFQMC correlation energies (inset) were computed for 4×4×1 meshes of k-points. Total energies are shown in the upper panel, measured from the minimum value, $E_{min} = E(R_{eq})$. The AFQMC equilibrium bondlengths are $R_{eq} = 1.5133(9), 1.4613(16), 1.4478(5), 1.4455(12)$ Å for GTH-SZV, GTH-DZV, GTH-DZVP and GTH-TZVP respectively; for reference, the reported experimental equi-

librium bondlength is $R_{eq} = 1.45$ Å [59].

So far, we have illustrated the use of symmetry when calculating total energies and lattice constants. We now briefly show that symmetry adaptation can be used when computing arbitrary ground-state properties in AFQMC, such as the electron density, within the back-propagation algorithm [11, 31, 40].

The electron density is computed by contracting the spin-summed one-body density matrix with the basis orbitals $\varphi_{p\mathbf{k}_p}(\mathbf{x})$, evaluated on a mesh of points $\mathbf{x}$ along the lattice plane,

$$\rho(\mathbf{x}) = \sum_{\substack{\mathbf{k}_p \mathbf{k}_q \\ pq\,\sigma}} \varphi^*_{p\mathbf{k}_p}(\mathbf{x})\varphi_{q\mathbf{k}_q}(\mathbf{x})\,\rho_{p\mathbf{k}_p,q\mathbf{k}_q} \quad . \tag{42}$$

The one-body density matrix is evaluated using the back-propagation algorithm as

$$\rho_{p\mathbf{k}_p,q\mathbf{k}_q} = \frac{1}{\sum_i W_i} \sum_i W_i \frac{\langle\Psi_i|\hat{a}^\dagger_{p\mathbf{k}_p}\hat{a}_{q\mathbf{k}_q}|\Phi_i\rangle}{\langle\Psi_i|\Phi_i\rangle} \quad . \tag{43}$$
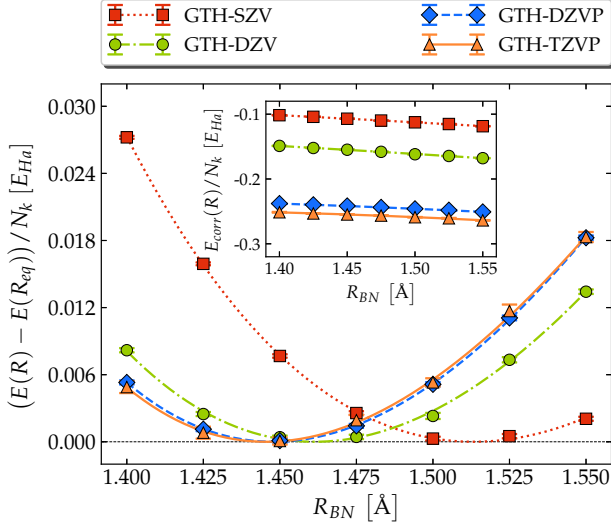
FIG. 5. AFQMC total (main figure) and correlation energy per cell (inset) of 2D hexagonal BN, for increasingly large basis sets, using a $4\times4\times1$ k-point mesh. Total energies are shown relative to the minimum value, attained at equilibrium bondlength, $E(R_{eq})$.
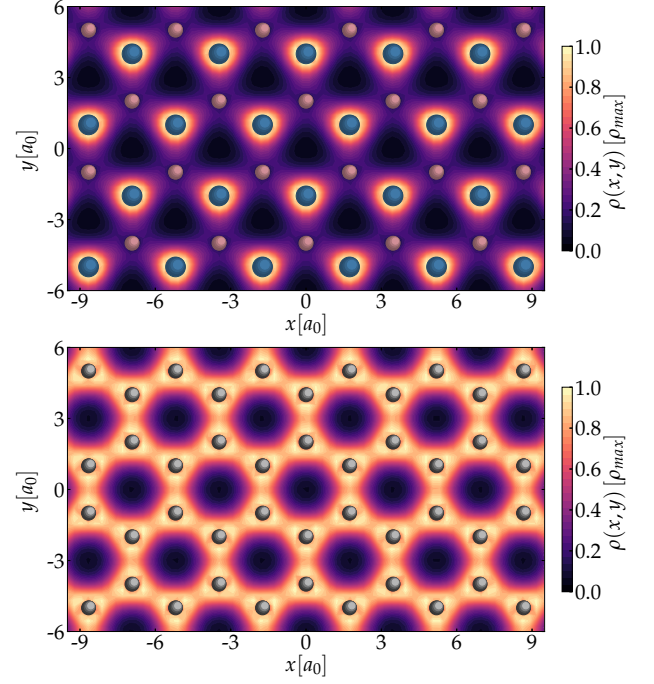

FIG. 6. AFQMC ground-state density of 2D hexagonal BN (top) and graphene (bottom) at the experimental equilibrium lattice constant a_0, using the GTH-DZV basis and GTH-Padé pseudopotential, along the lattice plane. Pink small (gray small, large blue) spheres denote B (C, N) atoms.

Here, $|\Psi_i\rangle$ is a stochastically sampled Slater determinant sampled at imaginary time $n\,\Delta\tau$, W_i its future weight at some time $(n+m)\,\Delta\tau$ and $\langle\Phi_i|$ is obtained back-propagating (i.e. propagating as a bra or linear functional, rather than a ket or vector) $\langle\Psi_T|$ along the segment of the future path of $|\Psi_i\rangle$, sampled during the time interval between $n\,\Delta\tau$ and $(n+m)\,\Delta\tau$ [40].

In Figure 6, we compute the electronic density of two low-dimensional materials, 2D hexagonal BN and graphene, within the GTH-DZV basis. The electron density illustrates the different nature of the two materials: while in graphene the density is distributed uniformly around C atoms, in BN there is a net concentration of electrons around N atoms, consistent with the charge-transfer nature of the material.

C. Timings

In Figure 7 we compare the timings of the standard and symmetry-adapted AFQMC implementations. Timings were performed on a cluster with Intel E5-2680, 2.4 GHz CPUs. In the various panels, the times for force bias and local energy evaluation, Hubbard-Stratonovich operator construction and walker propagation, the most expensive steps of an AFQMC calculation, are shown for standard AFQMC calculations of BN at the GTH-DZV level, using supercells of increasingly large size N_s, and symmetry-adapted calculations using k-point meshes of increasingly large size N_k. In a standard calculation, the local energy evaluation scales as N_s^4 and all the other subroutines as N_s^3. In a symmetry-adapted calculation, the local energy evaluation scales as N_k^3 and all the other

subroutines scale as N_k^2, confirming the reduction in scaling by one power arising from symmetry adaptation. In the current implementation, the lower scaling comes at the cost of an increased prefactor, so that crossover between the two strategies occurs around $N_s = N_k \simeq 10$ for the local energy evaluation and $N_s = N_k \simeq 20$ for all other subroutines.

V. CONCLUSIONS

In this work, we presented a formalism to perform AFQMC calculations that take advantage of Abelian Hamiltonian symmetries. We described how within a symmetry adapted orbital basis, the matrix elements of the Hamiltonian operator acquire block sparsity, which, when combined with a trial state that transforms as an irrep of the symmetry group and Hubbard-Stratonovich fields that also transform as irreps of the symmetry group, it is possible to reduce the cost and memory of the main steps in the AFQMC calculation by a factor of N_k^{-1}, where N_k is the order of the group.

Extending this formalism to non-Abelian symmetries is straightforward. The only difference arises because irreps of non-Abelian groups need not be one-dimensional. Thus products of objects that transform as irreps (such as $\varphi^*_{p\mathbf{k}_p}(\mathbf{r})\,\varphi_{r\mathbf{k}_r}(\mathbf{r})$) no longer simply transform as a single irrep $\mathbf{k}_r - \mathbf{k}_p$, but correspond to a linear combination of
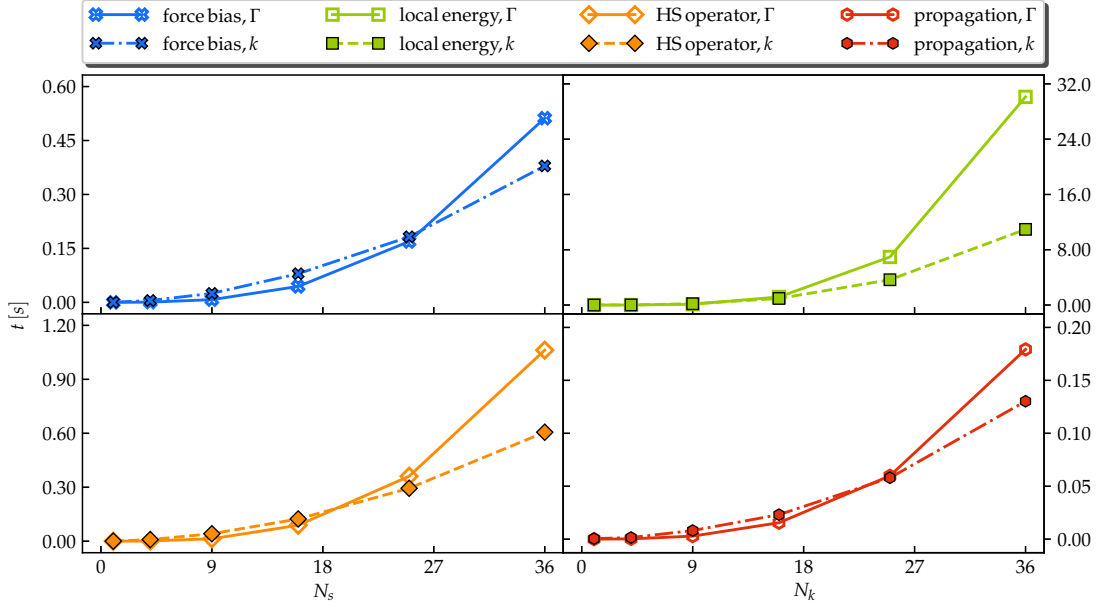
FIG. 7. (color online) Left to right and top to bottom: force bias (blue crosses), local energy (green squares), Hubbard-Stratonovich operator construction (orange diamonds) and walker propagation (red hexagons) times as a function of supercell size N_s (solid lines, empty symbols) or k-point mesh size N_k (dashed lines, filled symbols) for BN using the GTH-DZV basis and GTH-Padé pseudopotential.

objects, each transforming according to potentially different irreps. Nonetheless, all quantities that are block sparse in the current algorithm remain block sparse in the non-Abelian generalization, and a similar speedup of $\mathcal{O}(N_k^{-1})$ will be achieved as it is observed here.

As we showed in our demonstration calculations, the use of Abelian symmetries is particularly beneficial in the context of the large translational group associated with crystalline calculations. Thus we believe the present work will be particularly important in accelerating AFQMC calculations in realistic materials, and in particular, in removing finite size effects and in extrapolations to the thermodynamic limit.

VI. ACKNOWLEDGMENTS

Appendix A: Additional theoretical details

In Eq. (3) we introduced an M-dimensional matrix representation $\Gamma(\mathbf{s})_{rp}$ of the symmetry group $\mathcal{S}$. When symmetry operations are defined by functions $s : \mathbb{R}^3 \to \mathbb{R}^3$, then one has

$$\Gamma(\mathbf{s})_{rp} = \langle \varphi_r | \hat{\Gamma}(\mathbf{s}) | \varphi_p \rangle = \int_{\mathbb{R}^3} d\mathbf{x}\, \varphi_r^*(\mathbf{x})\, \varphi_p(s(\mathbf{x})) \quad . \quad \text{(A1)}$$

For example, for a translation by a vector $\mathbf{b}$, a rotation of an angle φ around an axis $\mathbf{n}$ and a reflection across a plane perpendicular to $\mathbf{v}$, one has

$$s(\mathbf{x}) = \mathbf{x} + \mathbf{b}\,,$$
$$s(\mathbf{x}) = \cos(\varphi)\,\mathbf{x} + \sin(\varphi)\,(\mathbf{n} \times \mathbf{x}) + \left(1 - \cos(\varphi)\right)\mathbf{n}(\mathbf{n} \cdot \mathbf{x})\,,$$
$$s(\mathbf{x}) = \mathbf{x} - 2\left(\mathbf{v} \cdot \mathbf{x}\right)\mathbf{v}\,.$$
$$\text{(A2)}$$

respectively.

1. Properties of the $\hat{\Pi}_{\mathbf{k}}$ operators

The relation

$$\sum_{\mathbf{k}} \frac{e^{-2\pi i \mathbf{k}\cdot\mathbf{s}}}{|\mathcal{S}|} = \prod_{i=0}^{r-1} \sum_{k_i=0}^{N_i-1} \frac{e^{-2\pi i \frac{k_i s_i}{n_i}}}{n_i} = \delta_{\mathbf{s},\mathbf{0}} \qquad \text{(A3)}$$

readily implies that the operators $\hat{\Pi}_{\mathbf{k}}$ are orthogonal projectors,

$$
\begin{aligned}
\hat{\Pi}_{\mathbf{k}}\hat{\Pi}_{\mathbf{k}'} &= \sum_{\mathbf{ss}'} \frac{e^{-2\pi i (\mathbf{k}\cdot\mathbf{s}-\mathbf{k}'\cdot\mathbf{s}')}}{|\mathcal{S}|^2}\hat{\Gamma}(\mathbf{s})\hat{\Gamma}(\mathbf{s}') \\
&= \sum_{\mathbf{st}} \frac{e^{-2\pi i \left(\mathbf{k}\cdot\mathbf{s}-\mathbf{k}'\cdot(\mathbf{t}-\mathbf{s})\right)}}{|\mathcal{S}|^2}\hat{\Gamma}(\mathbf{t}) \quad\quad (A4)\\
&= \sum_{\mathbf{s}} \frac{e^{-2\pi i \left((\mathbf{k}-\mathbf{k}')\cdot\mathbf{s}\right)}}{|\mathcal{S}|}\hat{\Pi}_{\mathbf{k}'} = \delta_{\mathbf{k},\mathbf{k}'}\hat{\Pi}_{\mathbf{k}'} \quad .
\end{aligned}
$$

Completeness holds, since

$$
\sum_{\mathbf{k}}\hat{\Pi}_{\mathbf{k}} = \sum_{\mathbf{sk}}\frac{e^{-2\pi i \mathbf{k}\cdot\mathbf{s}}}{|\mathcal{S}|}\hat{\Gamma}(\mathbf{s}) = \sum_{\mathbf{s}}\delta_{\mathbf{s},\mathbf{0}}\hat{\Gamma}(\mathbf{s}) = \hat{\mathbb{1}} \quad , \quad (A5)
$$

and the neutral element $\mathbf{0}$ of $\mathbb{Z}_{\mathcal{S}}$ is mapped onto the neutral element $\hat{\Gamma}(\mathbf{0}) = \hat{\mathbb{1}}$ of $\mathcal{S}$. Finally,

$$
\hat{\Gamma}(\mathbf{s})\hat{\Pi}_{\mathbf{k}} = \sum_{\mathbf{t}}\frac{e^{-2\pi i \mathbf{k}\cdot\mathbf{t}}}{|\mathcal{S}|}\hat{\Gamma}(\mathbf{s}+\mathbf{t}) = e^{2\pi i \mathbf{k}\cdot\mathbf{s}}\hat{\Pi}_{\mathbf{k}} \quad . \quad (A6)
$$

Hamiltonian sparsity easily follows from the fact that symmetry-adapted orbitals are eigenfunctions of projection operators, and that projection operators commute with the one-body and two-body parts of the Hamiltonian. Indeed,

$$
\begin{aligned}
\langle p\mathbf{k}_p|\hat{H}_1|q\mathbf{k}_q\rangle &= \langle p\mathbf{k}_p|\hat{\Pi}_{\mathbf{k}_p}\hat{H}_1|q\mathbf{k}_q\rangle \\
&= \langle p\mathbf{k}_p|\hat{H}_1\hat{\Pi}_{\mathbf{k}_p}|q\mathbf{k}_q\rangle = \delta_{\mathbf{k}_p\mathbf{k}_q}h_{pq}(\mathbf{k})
\end{aligned} \quad (A7)
$$

and, since the projectors onto symmetry adapted orbitals in the two-particle Hilbert space become

$$
\hat{\Pi}_{\mathbf{k}}^{(2)} = \sum_{\mathbf{k}_1}\hat{\Pi}_{\mathbf{k}_1}\otimes\hat{\Pi}_{\mathbf{k}-\mathbf{k}_1} \quad , \quad (A8)
$$

one has

$$
\begin{aligned}
(p\mathbf{k}_p r\mathbf{k}_r|q\mathbf{k}_q s\mathbf{k}_s) &= \langle p\mathbf{k}_p q\mathbf{k}_q|\hat{H}_2|r\mathbf{k}_r s\mathbf{k}_s\rangle \\
&= \langle p\mathbf{k}_p q\mathbf{k}_q|\Pi_{\mathbf{k}_p+\mathbf{k}_q}^{(2)}\hat{H}_2|r\mathbf{k}_r s\mathbf{k}_s\rangle \\
&= \langle p\mathbf{k}_p q\mathbf{k}_q|\hat{H}_2\Pi_{\mathbf{k}_p+\mathbf{k}_q}^{(2)}|r\mathbf{k}_r s\mathbf{k}_s\rangle \\
&= \delta_{\mathbf{k}_p+\mathbf{k}_q,\mathbf{k}_r+\mathbf{k}_s}(p\mathbf{k}_p r\mathbf{k}_r|q\mathbf{k}_q s\mathbf{k}_s) \quad .
\end{aligned} \quad (A9)
$$

2. Density fitting and Cholesky decomposition

In this Section we show how the structure (23) emerges when the electron-electron interaction is treated within the density fitting (DF) or Cholesky (CD) decomposition. Within DF, the electron repulsion integral is approximated by density fitting with an auxiliary basis of atom-centered Gaussian atomic orbitals $\{\chi_\gamma\}_{\gamma=1}^{N_\gamma}$,

$$
(pr|qs) \simeq \sum_{\gamma\delta}(pr|\gamma)S_{\gamma\delta}^{-1}(\delta|qs) \quad . \quad (A10)
$$

where $S_{\gamma\delta} = \langle\chi_\gamma|\chi_\delta\rangle$. The action of the symmetry group on the auxiliary basis $\{\chi_\gamma\}_\gamma$ is captured by a family of operators

$$
\hat{\Gamma}(\mathbf{s})|\chi_\gamma\rangle = \sum_\delta \Gamma(s)_{\gamma\delta}|\chi_\delta\rangle \quad , \quad (A11)
$$

so that, by following the procedure outlined in Section II A, one can produce an orthonormal basis of symmetry-adapted auxiliary basis functions $\tilde{\chi}_{\gamma\mathbf{Q}}$ (with overlap matrix equal to the identity). The electron repulsion integral reads, in the symmetry-adapted molecular and auxiliary bases,

$$
\frac{(p\mathbf{k}_r + \mathbf{Q}, r\mathbf{k}_r|q\mathbf{k}_s - \mathbf{Q}, s\mathbf{k}_s)}{2} = \sum_\gamma L^{\gamma,\mathbf{Q}}_{p\mathbf{k}_r+\mathbf{Q},r\mathbf{k}_r}L^{\gamma,-\mathbf{Q}}_{q\mathbf{k}_s-\mathbf{Q},s\mathbf{k}_s}
$$

$$(A12)$$

where summation is restricted to auxiliary basis functions belonging to the irrep labelled by $\mathbf{Q}$ for the pair $(p\mathbf{k}_r + \mathbf{Q}, r\mathbf{k}_r)$ and by $-\mathbf{Q}$ for the pair $(q\mathbf{k}_s - \mathbf{Q}, s\mathbf{k}_s)$ respectively.

Performing a Cholesky decomposition of the electron repulsion integral,

$$
\frac{(p\mathbf{k}_p r\mathbf{k}_r|q\mathbf{k}_q s\mathbf{k}_s)}{2} = \sum_\gamma L^\gamma_{p\mathbf{k}_p,r\mathbf{k}_r}L^\gamma_{q\mathbf{k}_q,s\mathbf{k}_s} \quad (A13)
$$

may not lead to the form (23), i.e. the tensor L may not be sparse. The desired structure can be extracted performing a SVD of the rank-three tensor $L^\gamma_{q\mathbf{k}_q,s\mathbf{k}_s} = \sum_\mu U^\mu_{q\mathbf{k}_q,s\mathbf{k}_s}\sigma_\mu V^{\mu\gamma}$ After the SVD is taken, the ERI reads

$$
\frac{(p\mathbf{k}_p r\mathbf{k}_r|q\mathbf{k}_q s\mathbf{k}_s)}{2} = \sum_\mu U^\mu_{p\mathbf{k}_p,r\mathbf{k}_r}\sigma_\mu^2 U^\mu_{q\mathbf{k}_q,s\mathbf{k}_s} \quad , \quad (A14)
$$

and the tensor U is non-zero only for certain values of the index μ, that depend only on the difference $\mathbf{k}_p - \mathbf{k}_r = \mathbf{Q}$. Indices μ can thus be parametrized as pairs $\gamma, \mathbf{Q}$, and the ERI takes the desired form in Sec. II A.

Appendix B: Additional algorithmic details

1. Interaction as squares of one-body operators

Starting from (10), we interchange the creation and destruction operators,

$$
\begin{aligned}
\hat{a}^\dagger_{p\mathbf{k}_r+\mathbf{Q}}\hat{a}^\dagger_{q\mathbf{k}_s-\mathbf{Q}}\hat{a}_{s\mathbf{k}_s}\hat{a}_{r\mathbf{k}_r} &= -\hat{a}^\dagger_{p\mathbf{k}_r+\mathbf{Q}}\hat{a}^\dagger_{q\mathbf{k}_s-\mathbf{Q}}\hat{a}_{r\mathbf{k}_r}\hat{a}_{s\mathbf{k}_s} \\
&= \hat{a}^\dagger_{p\mathbf{k}_r+\mathbf{Q}}\hat{a}_{r\mathbf{k}_r}\hat{a}^\dagger_{q\mathbf{k}_s-\mathbf{Q}}\hat{a}_{s\mathbf{k}_s} - \delta_{r\mathbf{k}_r,q\mathbf{k}_s-\mathbf{Q}}\hat{a}^\dagger_{p\mathbf{k}_r+\mathbf{Q}}\hat{a}_{s\mathbf{k}_s}
\end{aligned}
$$

$$(B1)$$

and inserting this equation in (10), obtaining

$$
\begin{aligned}
\hat{H} - E_0 = \\
\sum_{\mathbf{k}}\left(h_{pq}(\mathbf{k}) - \sum_{\mathbf{k}_r r}\frac{(p\mathbf{k}, r\mathbf{k}_r|r\mathbf{k}_r, q\mathbf{k})}{2}\right)\hat{a}^\dagger_{p\mathbf{k}}\hat{a}_{q\mathbf{k}} \\
+ \sum_{\gamma\mathbf{Q}}\hat{L}_{\gamma,\mathbf{Q}}\hat{L}_{\gamma,-\mathbf{Q}}
\end{aligned} \quad (B2)
$$

with $\hat{L}_{\gamma,\mathbf{Q}}$ as in Eq. (25). The one-body Hamiltonian now reads $\tilde{h}_{pq}(\mathbf{k}) = h_{pq}(\mathbf{k}) - \sum_{\mathbf{k}_r r} \frac{(p\mathbf{k}, r\mathbf{k}_r | r\mathbf{k}_r, q\mathbf{k})}{2}$ and, to obtain a representation as a sum of squares of one-body operators, we observe that

$$\sum_{\mathbf{Q}\gamma} \hat{L}_{\gamma,\mathbf{Q}} \hat{L}_{\gamma,-\mathbf{Q}} = \frac{1}{2} \sum_{\mathbf{Q}\gamma} \hat{L}_{\gamma,\mathbf{Q}} \hat{L}_{\gamma,-\mathbf{Q}} + \hat{L}_{\gamma,-\mathbf{Q}} \hat{L}_{\gamma,\mathbf{Q}} =$$

$$-\frac{1}{2} \left[\sum_{\mathbf{Q}\gamma} \left(\frac{i\hat{L}_{\gamma,\mathbf{Q}} + i\hat{L}_{\gamma,-\mathbf{Q}}}{\sqrt{2}} \right)^2 + \left(\frac{\hat{L}_{\gamma,\mathbf{Q}} - \hat{L}_{\gamma,-\mathbf{Q}}}{\sqrt{2}} \right)^2 \right]. \tag{B3}$$

2. Mean-field background subtraction

The mean-field background subtraction requires replacing the operators $\hat{L}_{\mathbf{Q},\gamma}$ with $\hat{L}'_{\mathbf{Q},\gamma}$ in (24). This leads to

$$\hat{H} - E_0 = \sum_\gamma \ell_\gamma^2 + 2 \sum_\gamma \ell_\gamma \hat{L}'_{\mathbf{0},\gamma}$$

$$+ \sum_{\substack{\mathbf{k}pq \\ \sigma}} \left(h_{pq}(\mathbf{k}) - \frac{1}{2} \sum_{\mathbf{k}_r r} (p\mathbf{k}, r\mathbf{k}_r | r\mathbf{k}_r, q\mathbf{k}) \right) \hat{a}^\dagger_{p\mathbf{k}} \hat{a}_{q\mathbf{k}}$$

$$-\frac{1}{2} \sum_{\mathbf{Q}\gamma} \left[\left(\frac{i\hat{L}'_{\gamma,\mathbf{Q}} + i\hat{L}'_{\gamma,-\mathbf{Q}}}{\sqrt{2}} \right)^2 + \left(\frac{\hat{L}'_{\gamma,\mathbf{Q}} - \hat{L}'_{\gamma,-\mathbf{Q}}}{\sqrt{2}} \right)^2 \right], \tag{B4}$$

where ℓ is defined as in Eq. (28). The operator (B4) has the same form as in (19) with $\hat{H}'_1 = \sum_{\mathbf{k}} h'_{pq}(\mathbf{k}) \hat{a}^\dagger_{p\mathbf{k}} \hat{a}_{q\mathbf{k}}$,

$$h'_{pq}(\mathbf{k}) = h_{pq}(\mathbf{k}) - \frac{1}{2} \sum_{\mathbf{k}_r r} (p\mathbf{k}, r\mathbf{k}_r | r\mathbf{k}_r, q\mathbf{k})$$

$$+ 2 \sum_\gamma \ell_\gamma L^{\gamma,\mathbf{0}}_{p\mathbf{k}, q\mathbf{k}} - \frac{\ell_\gamma^2}{N} \delta_{pq}, \tag{B5}$$

and $\hat{v}'_\gamma$ as detailed in the main text.

3. Reducing the number of auxiliary fields

by Lagrangian partition

In (24), the Hamiltonian was expressed as

$$\hat{H} = E_0 + \hat{H}'_1$$

$$-\frac{1}{2} \sum_{\mathbf{Q}\gamma} \left[\left(\frac{i\hat{L}'_{\gamma,\mathbf{Q}} + i\hat{L}'_{\gamma,-\mathbf{Q}}}{\sqrt{2}} \right)^2 + \left(\frac{\hat{L}'_{\gamma,\mathbf{Q}} - \hat{L}'_{\gamma,-\mathbf{Q}}}{\sqrt{2}} \right)^2 \right], \tag{B6}$$

clearly leading to $2N_\gamma$ auxiliary fields. This is more than in a calculation that does not incorporate symmetry. To reduce the number of auxiliary fields, we partition the irreps $\mathbf{Q}$ of the symmetry group into three sets:

- the set $\mathcal{P}_0 = \{\mathbf{Q} : \mathbf{Q} = -\mathbf{Q}\}$ of $\mathbf{Q}$ coinciding with their inverse

- any subset $\mathcal{P}_+ \subset \mathbb{Z}_\mathcal{S} - \mathcal{P}_0$ such that, if $\mathbf{Q} \in \mathcal{P}_+$, then $-\mathbf{Q} \notin \mathcal{P}_+$

- $\mathcal{P}_- = \mathbb{Z}_\mathcal{S} - \mathcal{P}_0 - \mathcal{P}_+$

According to Lagrange's theorem [27–29], the set $\mathcal{P}_0$ contains elements other than $\mathbf{0}$ in, and only in, groups with even order $|\mathcal{S}|$. Then clearly one has

$$\hat{H} = E_0 + \hat{H}'_1 - \frac{1}{2} \sum_{\mathbf{Q} \in \mathcal{P}_0, \gamma} \left(\sqrt{2} \hat{L}'_{\mathbf{Q},\gamma} \right)^2$$

$$-\frac{1}{2} \sum_{\mathbf{Q} \in \mathcal{P}_+, \gamma} \left[\left(i\hat{L}'_{\gamma,\mathbf{Q}} + i\hat{L}'_{\gamma,-\mathbf{Q}} \right)^2 + \left(\hat{L}'_{\gamma,\mathbf{Q}} - \hat{L}'_{\gamma,-\mathbf{Q}} \right)^2 \right]. \tag{B7}$$

Now, since $|\mathcal{P}_0| + 2|\mathcal{P}_+| = |\mathcal{S}|$, the interaction part of the Hamiltonian has been reduced to a sum of N_γ squares of one-body operators, the same as in a calculation that does not enforce symmetries.

With this representation of the Hamiltonian, the small-imaginary-time propagator has the form (35) with

$$\int d\mathbf{x}\, e^{\hat{A}(\mathbf{x})} = \int \prod_{\mathbf{Q} \in \mathcal{P}_0 \gamma} dx_{\mathbf{Q}\gamma 1} \prod_{\mathbf{Q} \in \mathcal{P}_+ \gamma} dx_{\mathbf{Q}\gamma 1} dx_{\mathbf{Q}\gamma 2}$$

$$e^{\sqrt{2\Delta\tau} \sum_{\gamma, \mathbf{Q} \in \mathcal{S}} i\, x_{\mathbf{Q}\gamma 1} \hat{L}'_{\gamma,\mathbf{Q}}}.$$

$$e^{\sqrt{\Delta\tau} \sum_{\gamma, \mathbf{Q} \in \mathcal{P}_+} i x_{\mathbf{Q}\gamma 1} \left(\hat{L}'_{\gamma,\mathbf{Q}} + \hat{L}'_{\gamma,-\mathbf{Q}} \right)}$$

$$e^{\sqrt{\Delta\tau} \sum_{\gamma, \mathbf{Q} \in \mathcal{P}_+} x_{\mathbf{Q}\gamma 2} \left(\hat{L}'_{\gamma,\mathbf{Q}} - \hat{L}'_{\gamma,-\mathbf{Q}} \right)}. \tag{B8}$$

This leads immediately to the form of the matrix $\mathcal{A}$ associated with $\hat{A}(\mathbf{x})$.

[1] M. Born and R. Oppenheimer, Annalen der Physik **389**, 457 (1927).

[2] J. Ziman, *Principles of the theory of solids* (University Press, 1965).

[3] A. Szabo and N. Ostlund, *Modern Quantum Chemistry: Introduction to Advanced Electronic Structure Theory*, Dover Books on Chemistry (Dover Publications, 1989).

[4] M. Dupuis and H. F. King, International Journal of Quantum Chemistry **11**, 613 (1977).

[5] J. F. Stanton, J. Gauss, J. D. Watts, and R. J. Bartlett,

The Journal of Chemical Physics **94**, 4334 (1991).

[6] G. K.-L. Chan and M. Head-Gordon, The Journal of Chemical Physics **116**, 4462 (2002).

[7] J. McClain, Q. Sun, G. K.-L. Chan, and T. C. Berkelbach, Journal of Chemical Theory and Computation **13**, 1209 (2017), pMID: 28218843.

[8] Q. Sun, T. C. Berkelbach, N. S. Blunt, G. H. Booth, S. Guo, Z. Li, J. Liu, J. D. McClain, E. R. Sayfutyarova, S. Sharma, S. Wouters, and G. K.-L. Chan, Wiley Interdisciplinary Reviews: Computational Molecular Science **8**, e1340.

[9] R. Blankenbecler, D. J. Scalapino, and R. L. Sugar, Phys. Rev. D **24**, 2278 (1981).

[10] G. Sugiyama and S. Koonin, Annals of Physics **168**, 1 (1986).

[11] S. Zhang, J. Carlson, and J. E. Gubernatis, Phys. Rev. B **55**, 7464 (1997).

[12] N. Rom, E. Fattal, A. K. Gupta, E. A. Carter, and D. Neuhauser, The Journal of Chemical Physics **109**, 8241 (1998).

[13] R. Baer, M. Head-Gordon, and D. Neuhauser, The Journal of Chemical Physics **109**, 6219 (1998).

[14] S. Zhang and H. Krakauer, Phys. Rev. Lett. **90**, 136401 (2003).

[15] W. A. Al-Saidi, S. Zhang, and H. Krakauer, J. Chem. Phys. **124**, 224101 (2006).

[16] S. Zhang, in *Emergent Phenomena in Correlated Matter: Modeling and Simulation*, edited by E. P. E. Koch and U. Schollwöck (Verlag des Forschungszentrum Jülich, 2013) Chap. 15.

[17] M. Motta and S. Zhang, WIREs Comput Mol Sci **e1364**, 1 (2018).

[18] R. Evarestov, *Quantum Chemistry of Solids: LCAO Treatment of Crystals and Nanostructures*, Springer Series in Solid-State Sciences (Springer Berlin Heidelberg, 2013).

[19] R. Dovesi, R. Orlando, A. Erba, C. M. Zicovich-Wilson, B. Civalleri, S. Casassa, L. Maschio, M. Ferrabone, M. De La Pierre, P. D'Arco, Y. Noël, M. Causa, M. Rerat, and B. Kirtman, International Journal of Quantum Chemistry **114**, 1287 (2014).

[20] G. H. Booth, T. Tsatsoulis, G. K.-L. Chan, and A. Grüneis, The Journal of Chemical Physics **145**, 084111 (2016).

[21] Q. Sun, T. C. Berkelbach, J. D. McClain, and G. K.-L. Chan, The Journal of Chemical Physics **147**, 164119 (2017).

[22] T. Gruber, K. Liao, T. Tsatsoulis, F. Hummel, and A. Grüneis, Phys. Rev. X **8**, 021043 (2018).

[23] C. Lin, F. H. Zong, and D. M. Ceperley, Phys. Rev. E **64**, 016702 (2001).

[24] F. Ma, W. Purwanto, S. Zhang, and H. Krakauer, Phys. Rev. Lett. **114**, 226401 (2015).

[25] S. Zhang, F. D. Malone, and M. A. Morales, The Journal of Chemical Physics **149**, 164102 (2018).

[26] F. D. Malone, S. Zhang, and M. A. Morales, Journal of Chemical Theory and Computation **15**, 256 (2019).

[27] T. W. Hungerford, *Algebra* (Springer, 1980).

[28] D. S. Dummit and R. M. Foote, *Abstract algebra* (New York: Wiley, 2004).

[29] W. Rudin, *Fourier Analysis on Groups* (Wiley, 1962).

[30] R. Jozsa, Proceedings of the Royal Society of London A: Mathematical, Physical and Engineering Sciences **454**, 323 (1998).

[31] W. Purwanto and S. Zhang, Phys. Rev. E **70**, 056702 (2004).

[32] J. Hubbard, Phys. Rev. Lett. **3**, 77 (1959).

[33] R. L. Stratonovich, Soviet Physics Doklady **2**, 416 (1958).

[34] J. P. F. LeBlanc, A. E. Antipov, F. Becca, I. W. Bulik, G. K.-L. Chan, C.-M. Chung, Y. Deng, M. Ferrero, T. M. Henderson, C. A. Jiménez-Hoyos, E. Kozik, X.-W. Liu, A. J. Millis, N. V. Prokof'ev, M. Qin, G. E. Scuseria, H. Shi, B. V. Svistunov, L. F. Tocchio, I. S. Tupitsyn, S. R. White, S. Zhang, B.-X. Zheng, Z. Zhu, and E. Gull (Simons Collaboration on the Many-Electron Problem), Phys. Rev. X **5**, 041041 (2015).

[35] M. Qin, H. Shi, and S. Zhang, Phys. Rev. B **94**, 235119 (2016).

[36] B.-X. Zheng, C.-M. Chung, P. Corboz, G. Ehlers, M.-P. Qin, R. M. Noack, H. Shi, S. R. White, S. Zhang, and G. K.-L. Chan, Science **358**, 1155 (2017).

[37] W. Purwanto, S. Zhang, and H. Krakauer, The Journal of Chemical Physics **142**, 064302 (2015).

[38] M. Motta, D. M. Ceperley, G. K.-L. Chan, J. A. Gomez, E. Gull, S. Guo, C. A. Jiménez-Hoyos, T. N. Lan, J. Li, F. Ma, A. J. Millis, N. V. Prokof'ev, U. Ray, G. E. Scuseria, S. Sorella, E. M. Stoudenmire, Q. Sun, I. S. Tupitsyn, S. R. White, D. Zgid, and S. Zhang (Simons Collaboration on the Many-Electron Problem), Phys. Rev. X **7**, 031059 (2017).

[39] J. Shee, B. Rudshteyn, E. J. Arthur, S. Zhang, D. R. Reichman, and R. A. Friesner, Journal of Chemical Theory and Computation **15**, 2346 (2019), pMID: 30883110.

[40] M. Motta and S. Zhang, Journal of Chemical Theory and Computation **13**, 5367 (2017), pMID: 29053270.

[41] M. Motta and S. Zhang, The Journal of Chemical Physics **148**, 181101 (2018).

[42] J. Shee, S. Zhang, D. R. Reichman, and R. A. Friesner, J. Chem. Theor. Comput. **13**, 2667 (2017).

[43] M. Motta, J. Shee, S. Zhang, and G. K.-L. Chan, (2018), arXiv:1810.01549.

[44] J. L. Whitten, The Journal of Chemical Physics **58**, 4496 (1973).

[45] E. G. Hohenstein and C. D. Sherrill, The Journal of Chemical Physics **132**, 184111 (2010).

[46] N. H. F. Beebe and J. Linderberg, International Journal of Quantum Chemistry **12**, 683 (1977).

[47] H. Koch, A. S. de Meras, and T. B. Pedersen, J. Chem. Phys. **118**, 9481 (2003).

[48] F. Aquilante, L. De Vico, N. Ferré, G. Ghigo, P.-A. Malmqvist, P. Neogrády, T. B. Pedersen, M. Pitoňák, M. Reiher, B. O. Roos, L. Serrano-Andrés, M. Urban, V. Veryazov, and R. Lindh, Journal of Computational Chemistry **31**, 224 (2010).

[49] W. Purwanto, H. Krakauer, Y. Virgus, and S. Zhang, J. Chem. Phys. **135**, 164105 (2011).

[50] G. C. Wick, Phys. Rev. **80**, 268 (1950).

[51] R. Balian and E. Brezin, Nuovo Cimento B **64**, 37 (1969).

[52] T. H. Dunning, The Journal of Chemical Physics **90**, 1007 (1989).

[53] D. E. Woon and T. H. Dunning, The Journal of Chemical Physics **98**, 1358 (1993).

[54] S. Goedecker, M. Teter, and J. Hutter, Phys. Rev. B **54**, 1703 (1996).

[55] C. Hartwigsen, S. Goedecker, and J. Hutter, Phys. Rev. B **58**, 3641 (1998).

[56] J. Hutter, M. Iannuzzi, F. Schiffmann, and J. VandeVondele, Wiley Interdisciplinary Reviews: Computa-

tional Molecular Science **4**, 15 (2014).

[57] H. Kwee, S. Zhang, and H. Krakauer, Phys. Rev. Lett. **100**, 126404 (2008).

[58] L. Schimka, J. Harl, and G. Kresse, The Journal of Chemical Physics **134**, 024116 (2011).

[59] https://github.com/cryos/avogadro/blob/master/crystals/nitrides/BN.cif.